Karlsruhe Institute of Technology

Institute of Mechanics

Numerical investigation of the effect of microscopic deformation mechanisms on the mechanical behavior of rubber-toughened ABS and PC/SAN multilayer materials

Juni 2009

Thomas Seelig

Institute of Mechanics
Kaiserstr. 12
D-76131 Karlsruhe
Tel.: +49 (0) 721/ 608-2071
Fax: +49 (0) 721/608-7990
E-Mail: info@ifm.kit.edu
www.ifm.uni-karlsruhe.de

Numerical investigation of the effect of microscopic deformation mechanisms on the mechanical behavior of rubber-toughened ABS and PC/SAN multilayer materials

Th. Seelig,
Institute of Mechanics, Karlsruhe University

Summary: The presentation deals with recent numerical investigations of the deformation and failure behaviour of heterogeneous amorphous polymers. Two classes of materials are considered, firstly ABS with rubber particles embedded in a glassy matrix and secondly composites with alternating layers of a brittle and a ductile glassy polymer. In both cases the overall response strongly depends on the interaction of plastic (shear) yielding and crazing on the micro-scale. Detailed finite element analyses are employed to study these interrelations.

Introduction

Amorphous glassy polymers are often given a heterogeneous microstructure in order to improve the materials overall ductility and fracture toughness. A typical example is ABS (acrylonitrile-butadiene-styrene) where submicron sized rubber particles are finely dispersed in a glassy matrix of SAN (styrene-acrylonitrile). While neat SAN subjected to tensile loading undergoes brittle failure by uncontrolled crazing at a few percent overall strain, the rubber particles in ABS serve to initiate dissipative micro-mechanisms (e.g. crazing) at many sites throughout the material (see Fig. 1a) so that much higher strains at failure and a larger amount of energy consumption are achieved, e.g. [1],[3],[4]. Though rubber-toughened materials such as ABS are well established since several decades, a detailed understanding of the relation between microstructure and overall response – necessary for tailoring materials with optimal properties – is still lacking. It seems, for instance, not entirely clear (and the reasons not understood) under which circumstances either matrix shear yielding or crazing is the dominant dissipative mechanism.

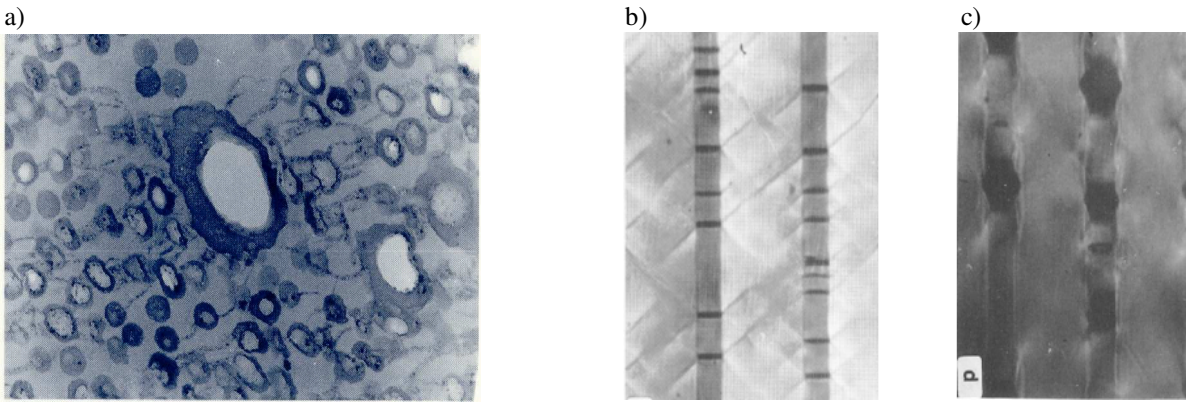

Figure 1: a) Microstructure of ABS showing crazes between voids which have formed from cavitated rubber particles [10]; b) PC/SAN multilayer composite under tensile loading parallel to layers showing a network of (diagonal) shear bands in the ductile PC layers and crazes/microcracks in the brittle SAN layers, c) microcracks in SAN layers have grown to holes at large overall strain [5]

Another class of materials where likewise the interplay between microstructure and microscopic deformation and damage mechanisms leads to an improved overall performance are multilayer composites obtained from co-extrusion a brittle (e.g. SAN) and a ductile (typically polycarbonate, PC) glassy polymer. Under tensile loading parallel to the layers (Fig. 1b and c), in these materials the unlimited growth of crazes (and subsequent cracks) formed in the brittle phase is prevented by the neighboring layers of the ductile phase. In the latter, shear bands are initiated which transfer stress concentrations to locations away from the initial defects. This leads to a network of crazes and shear bands which may extend over large regions of the material and gives rise to an enhanced overall ductility accompanied by a large amount of energy dissipation [5],[11].
A common feature of the two classes of materials is the coexistence of locally large plastic deformations (e.g. localized in shear bands) and crazing as two distinctly different micro-mechanisms. However, the situation is somewhat simpler in case of the PC/SAN multilayer composites in that these micro-mechanisms occur separately in the different constituents of the material, whereas in ABS they both occur in the SAN matrix around the rubber particles.
The computational models utilized here in order to gain some deeper understanding of the interrelation between microstructure, micro-mechanisms and overall behavior are the same in case of both classes of materials, i.e. detailed finite element models of the microstructure in conjunction with appropriate constitutive models and special cohesive elements capturing local separation processes (e.g. crazing). In view of the number of modeling assumptions and material parameters involved, the numerical studies of different materials presented in the sequel also provide some means of validation the numerical tools.

Constitutive models

The large strain rate-dependent deformation behavior of glassy polymers (sketched in Fig. 2a) is in the present work described using the material model developed in [2]. Beyond the range of small (linear) elastic strains the inelastic strain rate is given by

$$\boldsymbol{D}^{\mathrm{p}} = \dot{\gamma}_0 \exp\left(-\frac{As}{\theta}\left(1 - (|\bar{\boldsymbol{\sigma}}'|/s)^{5/6}\right)\right)\frac{\bar{\boldsymbol{\sigma}}'}{|\bar{\boldsymbol{\sigma}}'|} \qquad (1)$$

where $\bar{\boldsymbol{\sigma}} = \boldsymbol{\sigma} - \boldsymbol{b}$ denotes the driving stress, $(.)'$ its deviatoric part, and $s = s(\varepsilon^{\mathrm{p}}, p)$ is the athermal yield strength which depends on the accumulated plastic strain $\varepsilon^{\mathrm{p}} = \int \sqrt{\boldsymbol{D}^{\mathrm{p}} \cdot \boldsymbol{D}^{\mathrm{p}}}\, dt$ and on the hydrostatic pressure p. The temperature θ here is taken constant, and $\dot{\gamma}_0$ and A are material parameters. In order to describe the initial peak yield stress and the corresponding amount of subsequent softening, which depend on the thermal pre-history of the material (*physical aging*), the athermal yield strength s is taken to evolve with plastic strain from an initial value s_{o} down to a saturation value s_{s}.
Progressive rehardening due to stretching and alignment of the molecular network is described by the backstress tensor $\boldsymbol{b}$ computed according to a model from rubber (entropic) elasticity that accounts for a finite extensibility of molecular chains. More details along with values of the material parameters may be found e.g. in [10].

The formation of crazes and subsequent cracks in SAN is modeled utilizing a cohesive surface methodology developed in [12] and later on modified in [8]. The model represents the fibrillated craze matter and its stress-carrying capacity in a “smeared” sense by a separation

Δ_c of the craze-bulk interfaces (craze width) and a cohesive traction T. Upon craze initiation according to the criterion of a critical value of the maximum principal tensile stress, craze widening takes place at a rate $\dot{\Delta}_c$ which depends on the traction T related to the craze widening resistance σ_c:

$$\dot{\Delta}_c = \dot{\Delta}_0 \exp\left(\frac{A_c}{\theta}(T - \sigma_c) \right) \quad , \quad \sigma_c = \sigma_c(\Delta_c) \tag{2}$$

Here, $\dot{\Delta}_0$ and A_c are material constants and the craze widening resistance σ_c is taken to evolve with the craze thickness Δ_c as sketched in Fig. 2b. This non-monotonous variation reflects the different stages of the craze widening process as discussed in [8]. Finally, at a critical craze width Δ_c^{cr} the craze widening resistance (and consequently the cohesive traction T) drops to zero due to rupture of the craze fibrils and the craze (locally) turns into a crack.

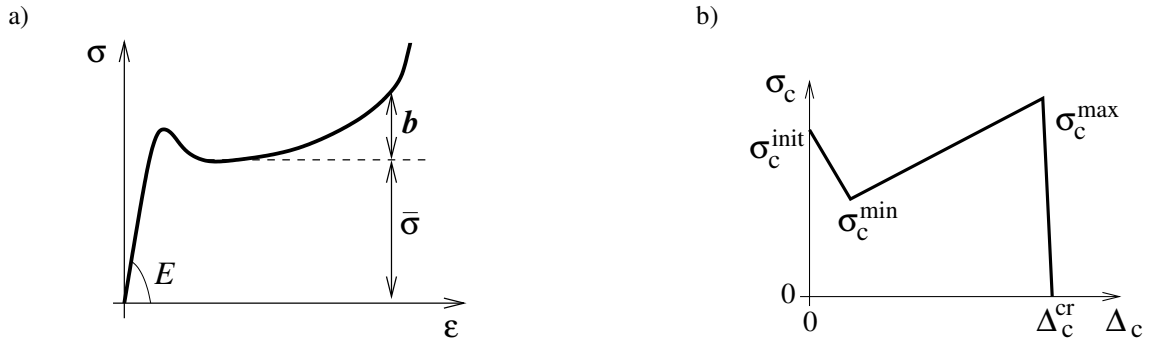

Figure 2: a) Uniaxial response of bulk glassy polymer in absence of crazing, b) variation of craze widening resistance with craze opening displacement (thickness) in cohesive model

Modeling ABS materials

The ABS microstructure is approximated here by a stacked hexagonal array of rubber particles embedded in the SAN matrix, subjected to loading in terms of macroscopic principal stresses along the symmetry axes (Fig. 3a). This morphology can be further approximated by a single axisymmetric unit cell (Fig. 3b). Since the rubber particles typically cavitate in the

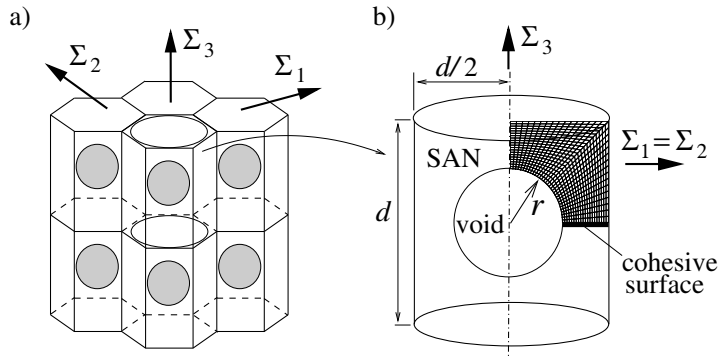

Figure 3: a) Model microstructure with rubber particles in SAN matrix arranged in stacked hexagonal array, b) axisymmetric unit cell model employed in numerical analysis

early stage of loading and thereafter have a negligible stiffness they are treated as voids. Crazes form as localized zones perpendicular to the direction of maximum principal stress. The latter coincides with the 3-direction in the present model by choosing $\Sigma_3 > \Sigma_1 = \Sigma_2$; hence crazing is expected to take place in the ring-shaped equator plane of the rubber particles (voids). The crazing process is described by means of the cohesive surface model outlined in the previous section. More details on this study may be found in [9].

Numerical results on ABS materials

Loading of the unit cell is imposed by prescribing velocities on the horizontal and vertical boundaries so that overall stress ratio $\Sigma_{1,2} / \Sigma_3$ is kept constant, and the overall axial strain rate is $\dot{\bar{\varepsilon}} = 1\ \mathrm{sec}^{-1}$.

For uniaxial overall loading Fig. 4 shows the macroscopic response of the unit cell for different values of the rubber content (porosity) f_0 and for two different values of the matrix initial yield strength s_o. Figure 4a with a value of $s_o = 95$ MPa corresponds to a "fresh" matrix material under quenched conditions (low stress peak and small amount of softening), whereas Fig. 4b with $s_o = 110$ MPa corresponds to a material which as experienced physical aging during annealing, known to result in a pronounced stress peak and softening. In the latter case the initial matrix yield stress is too high (compared to the craze stress) for matrix plasticity to take place, and the overall unit cell response reflects the bilinear craze response with an intermediate stress drop (at around 5% strain). For the lower initial yield stress underlying the results in Fig. 4a, however, matrix yielding takes place in the course of loading as can be seen from the nonlinear overall stress-strain response. Interestingly, the variation of failure strain with rubber content is contrary in the two cases; a decreasing failure strain with increasing rubber content is predicted when pronounced matrix shear yielding takes place (Fig. 4a).

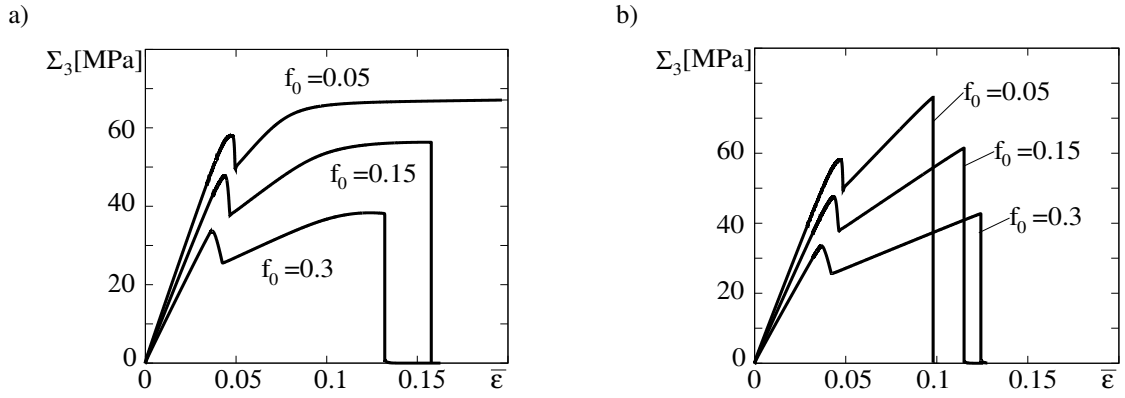

Figure 4: Effect of rubber content on unit cell response under overall uniaxial tension for matrix material with initial yield strength of a) s_o= 95 MPa (quenched conditions) and b) s_o = 110 MPa (annealed conditions)

Modelling PC/SAN multilayer composites

PC/SAN multilayer composites are modeled here assuming 2D plane strain conditions. A sample (of height h) of the material consisting of several layers as sketched in Fig. 5a is considered and overall loading parallel to the layers is imposed in terms of a prescribed velocity $\dot{u}$ on the upper boundary so that the macroscopic strain rate is $\dot{\bar{\varepsilon}} = \dot{u} / h$. Several

equally spaced cohesive surfaces normal to the loading direction are introduced throughout the sample as potential locations of failure (Fig. 5a). While failure in the SAN layers starts by the formation of crazes at a few per cent of strain, PC fails only after very large stretching of its molecular (entanglement) network is attained. This causes an incompatibility of the (continuum) deformation in the vicinity of the PC/SAN interface, and Figs. 5b-e illustrate how this is handled within the framework of the finite element model. More details on this study may be found in [8].

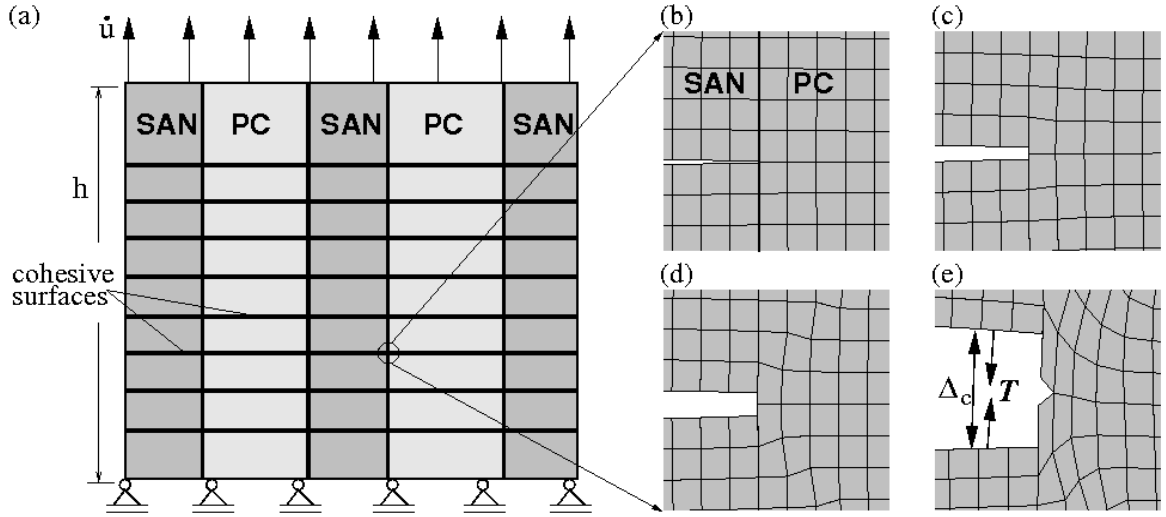

Figure 5: Micromechanical modeling of PC/SAN multilayer composites

Numerical results on multilayer composites

Two different multilayer composites, one with a PC/SAN composition (i.e. relative layer thickness) of 3/1 ("PC-rich") and one with a composition of 1/3 ("SAN-rich") are considered here, both under uniaxial overall loading. A spatially random distribution of initial defects is modelled by some scatter (±10%) of the local craze initiation stress in the SAN. Numerical results in terms of contours of the local plastic strain are shown for the PC-rich composite at two successive levels of overall deformation in Figs. 6a and b and for the SAN-rich composite in Fig. 6c. Plastic deformation starts by the formation of shear bands in the PC due to local stress concentrations induced by crazes in the SAN layers. When the shear bands impinge the neighboring PC/SAN interface, which in turn leads to a stress concentration in the SAN, new crazes are initiated there as can be seen from Figs. 6a and b. In a PC-rich composite this results in a network of interacting crazes and shear band extending uniformly throughout large regions of a test specimen (Figs. 6a and b). Even large holes in the SAN layers grown from former crazes with continued overall straining in this case are stabilized by the intermediate regions of ductile PC (Fig. 6b).

When the PC content (relative layer thickness) is low as in case of the PC/SAN (1/3) composite no such stable craze–shear band network is predicted from the simulations, rather a localisation of plastic deformation and damage is observed (Fig. 6c) leading to failure of the composite at low overall strain.

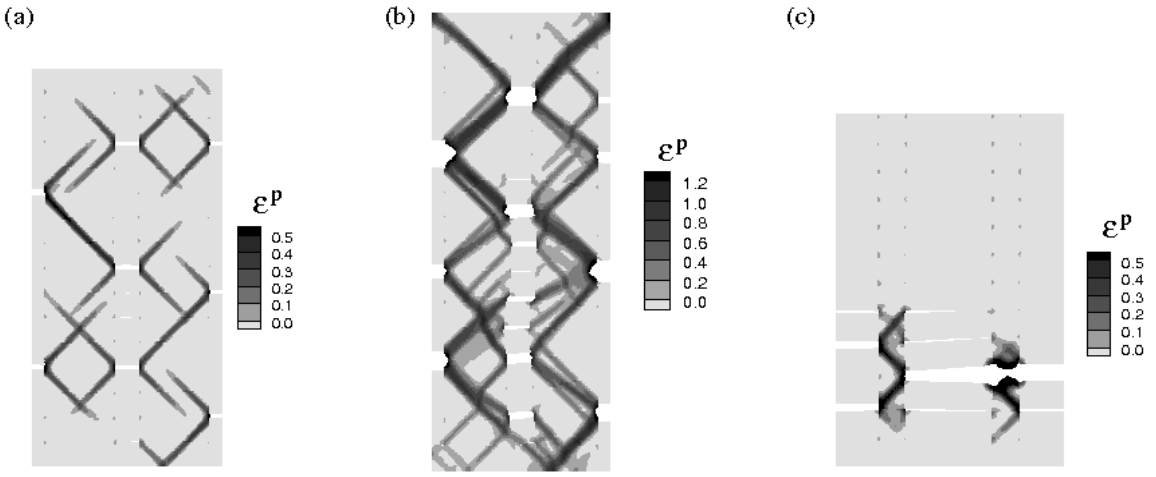

Figure 6: Patterns of local plastic deformation and damage in PC-rich composite (PC/SAN = 3/1) at a) 7 % and b) 20 % overall strain and in SAN-rich composite (PC/SAN = 1/3) at 7 % overall strain (c)

The overall response of the PC-rich and the SAN-rich composite is depicted in Fig.7 in terms of the macroscopic stress (loading of the sample) versus macroscopic strain. Here, results of several simulations with different, yet statistically equivalent, realisations of the initial defect distribution are included. Corresponding to the spatial extension of a network of interacting crazes and shear bands visible in Figs. 6a and b the PC-rich composites display a ductile overall behaviour. The SAN-rich composites, in contrast, undergo overall failure at small macroscopic strains due to the localisation of inelastic deformation shown in Fig. 6c.

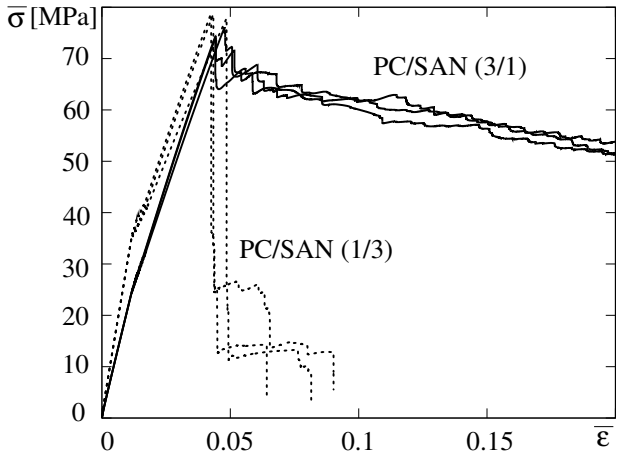

Figure 7: Overall response of PC-rich (3/1) and SAN-rich (1/3) composites under uniaxial tension; (a), (b), (c) correspond to contour plots in Fig. 6

Discussion and conclusions

In the present study employing an axisymmetric unit cell model of the microstructure of ABS materials and in an earlier study considering corresponding 2D plane strain models [7] the influence of some key material and microstructural parameters on the interaction between crazing and matrix yielding in rubber-toughened glassy polymers has been investigated. It turns out that, depending on the combination of these parameters, the overall response of the material (e.g. failure strain) may differ significantly. For instance, the dependence of the overall strain at failure on the rubber content may be strongly affected by the matrix yield behavior, as can be seen in Fig. 4. These observations have to be taken with some caution; they are partly artefacts of the simplified morphology considered so far. More realistic 3D microstructures, allowing for more complex void/craze interaction such as mutual shielding, therefore need to be investigated and are subject of ongoing research.

In case of PC/SAN multilayer composites the numerical results show a good qualitative agreement with experimental findings in [5] and [11]. This holds for the micro-scale deformation and damage mechanisms (craze-shear band network; see, e.g., Figs. 1b and 6a) as well as for the reproduction of the macroscopic brittle-to-ductile transition with increasing PC content. Quite similar results have recently been obtained from a more involved 3D study in [6].

Acknowledgment

Financial support of this work by the German Science Foundation (DFG) under Grant No. SE 872/5-1 is gratefully acknowledged.

References

[1] Bernal, C.R., Frontini, P.M., Sforza, M., Bibbo, M.A., *J. Appl. Pol. Sci.,* **1995**, 58, 1-10.
[2] Boyce, M.C., Parks, D.M., Argon, A.S., *Mech. Mater.* **1988**, *7*, 15-33.
[3] Bucknall, C.B., *Toughened Plastics*, Applied Science, London, **1977**
[4] Giaconi, G.F., Castellani, L., Maestrini, C., Ricco, T., *Polymer*, **1998**, 39, 6315-6324.
[5] Gregory, B.L., Siegmann, A., Im, J., Hiltner, A., Baer, E., *J. Mater. Sci.* **1987**, *22*, 532-538.
[6] Sharma, R., Boyce, M.C., Socrate, S., *Int. J. Solids Structures* **2008**, *45,* 2173-2202.
[7] Seelig, Th., Van der Giessen, E., in *Deformation und Bruchverhalten von Kunststoffen*, Merseburg, **2007**
[8] Seelig, Th., *Composites Science and Technology* **2008**, *68*, 1198-1208.
[9] Seelig, Th., Van der Giessen, E., *Computational Material Science* **2009**, *45*, 725-728.
[10] Steenbrink, A.C., *On Deformation and Fracture of Amorphous Polymer-Rubber Blends*; PhD thesis, Delft, **1998**
[11] Sung, K., Hiltner, A., Baer, E., *J. Mater. Sci.* **1994**, *29*, 5559-5568.
[12] Tijssens, M.G.A., Van der Giessen, E., Sluys, L.J., *Mech. Mater.* **2000**, *32*, 19-35.